

BIMA MILLIMETER-WAVE OBSERVATIONS OF THE CORE-JET AND MOLECULAR GAS IN THE FR I RADIO GALAXY NGC 3801

Mousumi Das¹, Stuart N. Vogel¹, Gijs A. Verdoes Kleijn², Christopher P. O'Dea^{3,4}, Stefi A. Baum^{3,5}

¹*Department of Astronomy, University of Maryland, College Park, MD 20742*

² *European Southern Observatory, Karl-Schwarzschild-Strasse-2, D-85748, Garching,
Germany*

³*Space Telescope Institute, 3700 San Martin Drive, Baltimore, MD 21218*

⁴ *Department of Physics, Rochester Institute of Technology, 84 Lomb Memorial Dr.,
Rochester, NY 14623-5603*

⁵ *Center for Imaging Science, Rochester Institute of Technology, 54 Lomb Memorial Dr.,
Rochester, NY 14623-5603*

email : mousumi@astro.umd.edu

ABSTRACT

We present BIMA 3 mm observations of the radio continuum source and the molecular gas disk in the radio loud Fanaroff & Riley Type I (FR I) galaxy NGC 3801. We have detected a continuum source in the nucleus and determined that it has a flat millimeter-wave spectrum, suggesting that the emission is non-thermal and due to an AGN; the radio core is not evident in existing VLA observations. We also map the extended 3 mm emission from the previously known radio jets. In addition, we detect CO (1–0) emission associated with the dust disk observed in previous HST images. A velocity gradient is observed, indicating a two kpc radius rotating gas ring or disk oriented roughly perpendicular to the radio jets. The inferred molecular gas mass of the disk is $M(H_2) = 3 \times 10^8 M_\odot$, about 1% of the dynamical mass. We also find a $\sim 10^8 M_\odot$ molecular gas clump not associated with the gas disk. There is evidence that this gas is associated with a merger and is infalling. This suggests that FR I type activity is related to merger activity, as is thought to be the case for FR II type radio galaxies. We also find indications that one of the radio jets is entraining gas from the infalling molecular gas.

Subject headings: galaxies:active — galaxies:individual (NGC 3801)— galaxies:ISM — interstellar:molecules — interstellar:kinematics and dynamics — radio lines:galaxies

1. INTRODUCTION

Radio loud galaxies are among the most energetic sources in the nearby universe. Associated with luminous early type (E/S0) galaxies, they often have relativistic jets originating in the nucleus near a supermassive black hole (SMBH) thought to power the enormous energy output (eg. Blandford 1984). Depending upon the jet morphology, the galaxies are classified as FR I (edge darkened) or FR II (edge brightened) sources (Fanaroff & Riley 1974). The core and jet structures have been mapped at various radio frequencies (e.g. Xu et al. 2000; Giovannini et al. 2005), from a few hundred MHz to several GHz. But radio continuum observations at millimeter wavelengths (~ 100 GHz) are relatively rare (Wright & Birkinshaw 1984; Salter et al. 1989; Evans et al. 1999a; Looney & Hardcastle 2000; Hardcastle & Looney 2001).

Molecular gas has been detected at millimeter wavelengths in several nearby radio loud galaxies (Lim et al. 2003; Leon et al. 2003; Lim et al. 2000; Evans et al. 1999a, 1999b; Mazzarella et al. 1993; Mirabel, Sanders & Kizes 1989; Philips et al. 1987); the mass of detected molecular gas is in the range $\sim 10^8$ – $10^{10} M_{\odot}$. The molecular gas mass is usually larger than that seen in radio quiet or normal ellipticals, where the gas mass appears in the range $\sim 10^8$ – $10^9 M_{\odot}$ (Lees et al. 1991; Wiklind, Combes & Henkel 1995; Knapp & Rupen 1996; Young 2002). Higher angular resolution observations which map and resolve the molecular gas distribution exist for only a few radio galaxies so far: Centaurus A (Eckart et al. 1990), 3C 84 (Inoue et al. 1996), 3C 293 (Evans et al. 1999a), PKS 1345+12 (Evans et al. 1999b) and 3C 31 (Okuda et al. 2005). These observations indicate that the gas is nearly always concentrated in a disk associated with the nuclear region. In at least one case (3C 293), the gas has a disturbed morphology (Evans et al. 1999a). The detection of large masses of molecular gas in radio galaxies and the location of this gas in the nucleus suggest that the gas provides a reservoir for fueling the AGN and powering the relativistically beamed jets.

However, many questions regarding jets in radio galaxies remain. For example, what is the origin of the gas feeding the AGN, how is the gas transported into the nuclear region, and what determines the luminosity of the AGN? X-ray observations indicate that radio galaxies can create bubbles and shells within the X-ray emitting gas in clusters of galaxies (e.g. Heinz,

Reynolds & Begelman 1998; Fabian et al. 2003). Thus jets from radio galaxies may play a significant role in heating the intracluster gas (see for example Reynolds et al. 2005 and references therein). The role of jets may be particularly prominent in less rich clusters or groups where gravitational heating is not as strong, and it is therefore of particular interest to observe jets and their interactions with gas in such systems.

To address some of these questions we have undertaken a study of molecular gas and millimeter continuum emission in several nearby radio loud galaxies. In this paper we present the first case in this study, NGC 3801 (UGC 06635). NGC 3801 is a nearby early type galaxy, variously classified as an elliptical or an S0 galaxy, located in a group of approximately ten galaxies; its basic properties are listed in Table 1. It is a radio bright galaxy with radio jets originating from the nucleus approximately normal to a central dust lane. It is classified as an FR I type radio source and has the classic edge-darkened jet structure typical of its class. The galaxy has been extensively imaged with the HST WFPC2 camera by Verdoes Kleijn et al. (1999). They find a prominent dust lane in the galaxy center with several associated filamentary structures; there are several knots of H α emission along the main dust lane that likely trace star forming regions. The radio jets have been mapped with the VLA at 1.5 GHz (Wrobel & Condon 1989); they extend out to a distance of $\sim 20''$ from the nucleus. The radio core is not detected with the VLA. HI has been detected toward NGC 3801 using the Arecibo radio telescope, with a total estimated HI mass of $2.1 \times 10^9 M_{\odot}$ (Heckman et al. 1983; Duprie & Schneider 1996). Leon et al. (2003) detected molecular gas in the center of NGC 3801; their single dish CO observations show that the line profile has a horn-shaped structure indicative of gas rotating in a disk or torus. They estimate a molecular gas mass of $\sim 3.8 \times 10^8 M_{\odot}$ in their $21''$ beam. We adopt a distance of $D = 47.9$ Mpc for NGC 3801 ($V_{sys} = 3451$ km s $^{-1}$), which leads to a scale of 0.23 kpc arcsec $^{-1}$.

In this paper we present a map of the molecular gas distribution in NGC 3801 using the BIMA millimeter-wave array. We have also detected the compact radio core in the center of the galaxy, which was not detected in lower frequency VLA observations. We have investigated the continuum emission at two other frequencies in the 3 mm window to determine whether the core emission has a flat or steep spectrum. This will help to understand whether the continuum emission is from an AGN.

2. OBSERVATIONS, DATA REDUCTION, AND MAPS

We observed NGC 3801 with the BIMA interferometer (Welch et al. 1996) in the C and D configurations from 2003 July to 2003 September. The observations were all obtained in single-pointing mode with a $100''$ field of view centered on the galaxy nucleus. The 114.2

GHz frequency of redshifted CO (1–0) was positioned in the upper sideband. We used the wideband correlator setting, which gives a velocity resolution of 50 km s^{-1} and a velocity range of $\sim 2000 \text{ km s}^{-1}$, covering 2100 to 4055 km s^{-1} ; this setting gives a lower velocity resolution than narrow band modes, but the large velocity width enables subtraction of the continuum emission to obtain a map of CO (1–0) line emission alone. We used the quasar 3C 273 for flux calibration. The flux of 3C 273 is monitored regularly with BIMA and varied by approximately 10% during the period of observation; additional errors are introduced when the flux calibration is transferred to the source. So the total error in the flux estimate is of the order of 10 to 20%. The radio source 1159+292 was used for phase calibration. Emission in the wideband channels is sufficiently bright that it could be used to self-calibrate the instrumental phases; self-calibration produced modest improvement in the images, and was used for the maps produced here. All interferometric data obtained with BIMA were reduced using MIRIAD (Sault, Teuben & Wright 1995).

2.1. 3 mm Continuum Emission and Spectral Index Maps

To obtain the continuum emission map, we flagged channels containing CO (1–0) line emission and recomputed the continuum channels from the narrow band dataset. We then averaged the upper sideband ($\sim 114.3 \text{ GHz}$) and the lower sideband ($\sim 110.6 \text{ GHz}$). The mean frequency of the continuum emission map is thus 112.4 GHz, corresponding to a wavelength of 2.7 mm. Figure 1 shows two maps of the distribution of 2.7 mm continuum emission in NGC 3801. Both maps combine data from the C and D arrays, but the map in the left panel is optimized for maximum sensitivity and flux recovery (using natural weighting) and the other compromises sensitivity slightly to achieve better resolution (using $\text{robust}=0.5$ weighting). The synthesized beam full width at half maximum diameters are $12 \times 10''$ and $10 \times 8''$, respectively.

To derive the spectral index of mm-wave continuum emission, we carried out additional BIMA observations at two new frequencies, 86 and 110 GHz. Although the 110 GHz frequency is not very different from the 112.4 GHz frequency used for the maps shown in this paper, we decided to observe two frequencies simultaneously so as to minimize the effect of calibration uncertainties, including those resulting from flux variations of the quasar used for flux calibration. We observed at 110 GHz rather than 112.4 GHz because the sensitivity improves away from the atmospheric oxygen band just beyond the CO (1–0) line. The spectral index observations were obtained in 2003 November using the C array in single-pointing mode with the wideband correlator setting. In order to use the same beam size for all frequencies, in making the spectral index maps we restricted the uv range of the visibilities

to the same range, $2 \text{ k}\lambda$ to $31 \text{ k}\lambda$. We used natural weighting. Even with the uv range restriction, the beam sizes were slightly different, and so we convolved all maps to the lowest resolution, $13.0'' \times 7.5''$.

Also, we used VLA 20 cm (1.5 GHz) archival data and our BIMA 2.7 mm map to determine the spectral index between millimeter and centimeter wavelengths. The highest resolution VLA map has a resolution of $1.5''$ and is shown in the upper left of Figure 2 and was obtained by Wrobel & Condon (1989). The faint diagonal striping is probably an artifact of incomplete uv coverage in the A array; the bend in both jets is not an artifact. In the upper right, we show a VLA B array 20 cm map at $4''$ emission that has been convolved to match the $10 \times 8''$ of the BIMA 2.7 mm map shown in Figure 1b.

2.2. CO (1–0) Emission

For the CO line emitting gas distribution, we need to subtract the continuum emission. As noted earlier, CO was observed in the upper sideband. The continuum maps presented in Figure 1 contain emission from the lower side band and so were not used. Instead, we formed a continuum map from off-line channels (2100 to 2900 km s^{-1}) in the upper sideband, and used that for continuum subtraction. The velocity-integrated CO (1–0) emission map, formed by taking the zeroth moment of the emission, is shown in Figure 3. Flux from pixels with absolute value less than 9 mJy beam^{-1} (1.1σ) was not included in the map shown. We note that clipping results in some of the flux being excluded from the map, and so in computing fluxes we used unclipped maps. The resolution of the natural-weighted map is $12'' \times 10''$.

3. RESULTS

3.1. Radio Continuum Core and Jet Emission

The distribution of 2.7 mm (114 GHz) continuum emission is shown in Figure 1. As described in Section 2.1, the right panel shows a robust-weighted map ($10 \times 8''$), while the left panel shows a natural-weighted map with slightly lower resolution ($12 \times 10''$) but with better sensitivity. The total 2.7 mm flux in the natural-weighted map is 51 mJy. The maps reveal that the source has both an unresolved core and extended structure.

In Figure 4, the natural-weighted 2.7 mm map (contours) is overlaid on the A-array VLA 20 cm (1.5 GHz) image. Here it can be seen that the 2.7 mm extended emission is

similar in position angle ($PA \sim 120^\circ$) and extent (radius $\sim 15''$) to the jet-like distribution evident in the 20 cm data. Although there is also 20 cm emission at the position of the 2.7 mm core, it is possible that this is entirely due to the jets. A radio core source has not previously been noted in NGC 3801; in particular, Xu et al. (2000) used VLA data taken by Wrobel and Condon to set an upper limit of 0.8 mJy on the 20 cm flux of the core source.

First we discuss the extended emission. Xu et al. (2000) classified NGC 3801 as a twin jet source on the basis of the centimeter wave VLA data, and noted that twin jet or core-jet structures are common in FR I radio galaxies. However, at millimeter wavelengths jets have only been detected in a few radio galaxies (e.g. Cygnus A: Wright & Birkinshaw 1984; 3C20: Hardcastle & Looney 2001; M87: Salter et al. 1989). Our detection of a core-jet structure in the FR I galaxy NGC 3801 at millimeter wavelengths is thus an important step in understanding of radio galaxies.

The curvature in the jets at 20 cm is also faintly seen in the BIMA 2.7 mm map. The curvature may indicate that the jets are precessing or deflected by irregularities in the interstellar medium of the galaxy (e.g. Merritt & Ekers 2002; Schmitt et al. 2002; Caproni & Abraham 2004; Hardee et al. 1994). In Figure 6, we overlay the VLA 20 cm map (contours) on the HST V-band image obtained by Verdoes Kleijn et al (1999). As noted by Verdoes Kleijn et al., the jets are at a position angle (PA) of 120° , roughly perpendicular to the disk-like dust filament at $PA=24^\circ$ passing near the nucleus. The figure also shows that the peak emission in the SE jet appears to coincide with the innermost extent of the long, well defined SE dust filament. We discuss this association further in Section 3.2.

In order to determine the cm to mm wave spectral index of the jets, we convolved the $1.5''$ 20 cm VLA map to the $10 \times 8''$ resolution of the BIMA 2.7 mm (112.4 GHz) map, as described in Section 2. The smoothed 20 cm map is shown in Figure 2 (upper right); a spectral index map formed from the ratio of the 2.7 mm map to the 20 cm map is shown in the lower left of the figure. The spectral index is -0.77 at the SE peak of cm-wave emission and -0.75 at the NW peak; it lies close to these values everywhere except closer to the nucleus where core emission contaminates jet emission, and near the edges where the signal to noise is not as good. The spectral index is similar to those measured in samples of FR I sources at much longer wavelengths (e.g. Parma et al. 1999), and is further discussed in Section 4.

Now we return to the millimeter-wave core source. As previously noted, this source was classified as a “twin-jet” source, not a “core-jet” source, by Xu et al. (2000) on the basis of the existing $1.5''$ 20 cm VLA data. Among their sample of ~ 20 nearby low-luminosity FR I radio galaxies, NGC 3801 has the third highest VLA 20 cm flux from the core-jet region. Yet it is among three galaxies in their sample with no detection of a core source, with an upper

limit for the core source of 0.8 mJy, an order of magnitude below the 17 core detections.

At 2.7 mm, the core is very clearly detected, with a S/N of 18 at the peak position in the natural-weighted map (Figure 1). Within the errors (estimated at $1''$ for the BIMA map), the position of peak 2.7 mm emission coincides with the nuclear position given in the near-IR 2MASS galaxy catalog (Jarrett et al. 2003), as shown in Figure 1. The flux at the position of the nucleus in the higher resolution $10 \times 8''$ map, which better resolves the core, is $18.0 \text{ mJy beam}^{-1}$. However, there is likely to be some contamination from jet emission. One way to separate unresolved emission from more extended emission is in the *uv* plane; however, the signal to noise is not sufficient for this. Instead we use the 20 cm map, which is completely dominated by jet emission, to estimate contamination from the jets. The spectral index map shows that the ratio of jet emission at 20 cm to that at 2.7 mm is very close to 27 everywhere (corresponding to a spectral index of -0.77). We divided the 20 cm map shown in the upper right of Figure 2 by this factor and subtracted the scaled 20 cm map from the 2.7 mm map. The result is shown in the lower right of Figure 2. Here it can be seen that contamination from jet emission has been cleanly removed. The slight extension at a position angle of about 20° , perpendicular to the jets, is probably not real. The flux in the 2.7 mm map, after subtracting the jets, is 15 mJy. Since the upper limit for the core at 20 cm is 0.8 mJy, we find that the core is at least 19 times brighter at 2.7 mm, corresponding to a spectral index greater than 0.68.

To learn more about the core source, we can investigate its spectral index over the range of wavelengths observable within the 3 mm atmospheric window. Figure 8 shows the core flux at several frequencies in the 3 mm window. Note that as described in Section 2 these observations were convolved to a common resolution of $13 \times 7.5''$, somewhat larger than that used for the core flux estimate at 2.7 mm, and so there is contamination from the jets at the 20% level. Also, because the map contains data only from the C array, some flux is resolved out, resulting in somewhat lower fluxes than in the D plus C array maps shown in Figure 1. Figure 8 shows that the 3 mm spectrum is flat to within the errors.

Figures 1 and 2 (lower right) show that the 2.7 mm continuum peak appears to lie about $1''$ east of the nuclear position given by the 2MASS near-IR peak (Jarrett et al. 2003); note that the 2MASS position is very close to the peak in the HST V-band image (Verdoes Kleijn et al. 1999). The absolute positional accuracy of interferometers such as BIMA is typically about 10% of the synthesized beam width. Since the beam is about $10''$, we expect a positional accuracy of about $1''$. The errors in the 2MASS position should be smaller than this. Therefore the millimeter-wave continuum and line observations presented here should be shifted about $1''$ west for accurate registration with the optical images shown in this paper.

3.2. CO (1–0) LINE EMISSION

The map of CO (1–0) velocity-integrated emission from a region $80''$ (18 kpc) on a side centered on NGC 3801 is shown in Figure 3; Figure 6 (lower panel) shows the same CO emission contours overlaid on the HST V-band image. The CO emission appears distributed in three main clumps, each labeled in Figure 3. The HST V-band image shows a straight prominent dust lane, measured to have a position angle (PA) of 24° by Verdoes Kleijn et al. (1999), which is offset approximately $1''$ west of the nucleus. CO clump A appears associated with the prominent NE extension of this filament. CO clump B is roughly coincident with the SW filament, although it appears offset by a couple of arc seconds to the east. It is possible that this offset is simply a result of low signal to noise. However, we note that the CO brightnesses of clumps A and B are similar but the SW dust filament is not as dark; this suggests the clump B gas may be located more towards the far side of the galaxy. Also, the major axis of the gaseous disk passes through the nucleus as might be expected, in contrast to the dust filament. We discuss the geometry of the nuclear disk later in the next section.

Clump C also appears to be associated with a dust filament: it peaks near the inner end of the well defined east filament that is oriented perpendicular to the filament associated with clumps A and B. The signal to noise is too low to determine whether the clump is extended.

The entire CO (1–0) emitting complex extends over nearly $\sim 30''$, with the peaks of clump A and B emission separated by about $20''$. Assuming a distance of 47.9 Mpc for NGC 3801, the molecular gas extends over a region nearly ~ 7 kpc across, with the peaks of the A and B clumps separated by approximately 4.6 kpc. The spectrum of the $30 \times 40''$ region centered on the nucleus is shown in Figure 5; emission is detected over a range of about 600 km s^{-1} .

The velocity-integrated CO (1–0) fluxes (S_{CO}) of the three clumps are similar, and are listed in Table 3. Together, the clumps total to $S_{CO} = 14.2 \text{ Jy km s}^{-1}$; this is similar to the flux measured by Leon et al. (2003) in the $21''$ IRAM 30-m single-dish beam. Some of the emission we detect is near the half-power response of the 30-m beam, and so the Leon et al. estimate is probably a lower limit to the total flux. We note in particular that our spectrum is more asymmetric than the Leon et al. spectrum. This might be explained if the IRAM beam was missing proportionally more of clumps B and C. However the BIMA map may be underestimating the total flux. This is because interferometric estimates of total flux tend to miss weak emission (see Helfer et al. 2002 and Helfer et al. 2003 for a discussion of this). To convert the CO fluxes to molecular mass, we use the standard conversion factor giving the molecular mass as $M_{mol} = 1.5 \times 10^4 D_{Mpc}^2 S_{CO} \text{ M}_\odot$, where D_{Mpc} is the distance in Mpc and S_{CO} is the velocity-integrated CO flux in Jy km s^{-1} (e.g. Strong et al. 1988;

Scoville et al. 1987). Note that this formula includes a factor of 1.36 for helium. We thus find that the three clumps, A, B, C, have masses 1.3, 1.7 and $1.8 \times 10^8 M_\odot$ (Table 3); since the interferometer may miss some of the flux, these estimates should probably be considered lower limits.

Figure 9 shows CO position-velocity contour plots for two cuts through the nucleus. The upper panel shows a cut at $PA=24^\circ$, parallel to the dust lane passing near the nucleus. This cut passes near the peaks of clumps A and B, which are labeled in the figure. Clump A has emission at velocities from 3180 to 3340 km s^{-1} ; clump B emits from 3580 to 3750 km s^{-1} . The figure shows a velocity jump between clumps A and B and a velocity gradient within clump B, suggesting rotation. We discuss the evidence that this is a rotating nuclear disk in Section 4.2. The lower panel shows a cut perpendicular to the first ($PA=114^\circ$), also through the nucleus. Clump C appears in this cut, with emission in the range 3470 to 3630 km s^{-1} .

To interpret these velocities, we need to know the systemic velocity of the galaxy. Values given in the literature for the redshift of NGC 3801 show a wide range; NED lists seven redshifts, in the range 3230 to 3460 km s^{-1} . However, not all of these are of similar quality. The Arecibo spectrum in DuPrie and Schneider (1996) is well determined with a good baseline. They report a systemic velocity of 3451 km s^{-1} . Their spectrum also shows absorption in the profile. The absorption, spectral baselines of limited extent, and confusion from other galaxies in the group may have confused some earlier HI observations. Given the fact that some of the HI may be due to merging gas and that existing HI observations do not resolve the galaxy, it is important to have confirming estimates of the systemic velocity using stellar tracers. A recent determination by Wegner et al. (2003), based on stellar absorption lines using a cross-correlation technique, gives a velocity of 3494 km s^{-1} , with an error of 70 km s^{-1} . This should avoid the uncertainties resulting from merging or asymmetrically distributed gas, since this determination is based on stars near the galaxy center. Similarly, the redshift for the Updated Zwicky Catalog used for the CfA survey is 3456 km s^{-1} with an error of 71 km s^{-1} . We adopt a systemic velocity of 3451 km s^{-1} , the estimate from the Arecibo HI spectrum.

The velocity extent of CO emission is very similar to that of the HI 21 cm profile observed by DuPrie and Schneider (1996). Also, the HI spectrum is in absorption in the velocity range 3460 to 3600 km s^{-1} , which corresponds closely to the velocity range of clump C (approximately 3470 to 3630 km s^{-1}). As mentioned earlier, the C component coincides with the inner part of the eastern dust filament (Figure 6); the large extinction implies that the dust filament and therefore the CO associated with it is on the near side of NGC 3801. We note also that this gas is along the line of sight to the SE radio continuum jet, as seen

in Figures 6 and 7. As is also evident in the figures, the 20 cm radio continuum comes almost entirely from the twin radio jets; therefore the 21 cm absorption must be produced by gas on the line of sight to the jets. This is very likely to be HI gas in the eastern dust filament, given its overlap with the SE radio jet. The fact that the HI absorption and clump C velocities are similar further increases the likelihood of this association, since the clump C coincides with the filament. We therefore conclude that the clump C is associated with the east dust filament, which is on the near side of NGC 3801, and that this filament produces the absorption seen in HI. Although the similarity in the position of clump C with the peak of the SE radio jet suggests a physical association, it is unclear whether this is the case. We discuss this further in the next section.

4. DISCUSSION

4.1. Nature of the AGN Core and Jets

Our BIMA detection of \sim 3 mm continuum emission from the core and jets in NGC 3801 is one of the key results of this paper, because radio cores and lobes have been detected at millimeter wavelengths in so few galaxies to date. Our 3 mm continuum observations reveal a bright radio core (Figure 1) which was not detected in 20 cm VLA observations (Figure 4). In the sample of 17 FR I galaxies studied by Xu et al. (2000), NGC 3801 was the only galaxy that lacked a VLA core and was hence not observed with the VLBA. One possible explanation for the absence of a core source is Doppler deboosting, which occurs for relativistic jets in the plane of the sky; the jets in NGC 3801 are probably close to the plane of the sky, given the similarity in fluxes from the two jets even close to the source and also the edge-on orientation of the nuclear disk. However, our BIMA observations clearly show that NGC 3801 has a bright radio core at 3 mm. This implies that the weakness of centimeter-wave emission from the core cannot be attributed to deboosting. Instead it is likely that the core is compact and dense. Synchrotron self absorption scales as ν^{-3} (e.g. Krolik 1999) and can explain the absence of centimeter-wave emission. At higher frequencies such as the 86–114 GHz frequencies observed here, the compact core is optically thin and thus appears bright. Synchrotron self absorption has also been observed in other radio cores (e.g. Rudnick, Jones & Fiedler 1986). Free-free absorption is also a possibility, but so far it is rarely seen in radio galaxies and even then seems to absorb only part of the inner regions (e.g., Walker et al. 2000; Jones et al. 2001). However, the absence of optical emission suggests that free-free absorption is also a plausible mechanism to explain the absence of centimeter wave emission from the core.

We find that the core spectrum is flat in the 3 mm window (86–114 GHz) (Figure 8 and

Table 2). Using the error limits on the peak fluxes at 86 GHz and 112.4 GHz, the range for the spectral index could however be -0.1 to -0.9. But after including the emission at 110 GHz, Figure 8 shows the core spectrum to be nearly flat. Steeply positive spectral indices, such as produced by dust emission (e.g. Wolfire & Churchwell 1994), are excluded. Optically thin free-free emission, such as might be produced by H II regions in a starburst, could produce a flat spectrum. However, the upper limit of 0.8 mJy on the 20 cm core flux rules out this possibility. The continuum flux from nuclei of starburst galaxies becomes higher with increasing wavelength at wavelengths greater than 2 cm (due to non-thermal emission), but shortward of 2 cm free-emission is optically thin (e.g. Turner and Ho (1983)). This means that the free-contribution at 3 mm must be well below 0.8 mJy, which is much less than the observed 15 mJy. We therefore conclude that the 3 mm continuum emission cannot be attributed to a starburst. Since flat millimeter-wave spectrum cores are often produced by non-thermal emission in other types of AGN than those in FR I galaxies, we conclude that the core emission is likely produced by an AGN. The flatness of the spectrum implies that we are seeing a compact source which is optically thick at 3mm. However the source may have a range of size scales, like a jet with some opening angle so that different parts of the structure become optically thin at different wavelengths (e.g., Blandford & Konigl 1979; Marscher 1980; Ghisellini & Maraschi 1989).

The bright, compact core and twin jet structure of NGC 3801 lend support to the idea that FR I sources are the parent population of BL Lac objects (Trussoni et al. 2003; Urry & Padovani 1995). According to this hypothesis, BL Lac radio sources are FR I nuclei in which the line of sight coincides with the axis of the radio jets; the resultant relativistic beaming effect produces very luminous radio cores. In NGC 3801, the twin jet structure indicates a large beaming angle. But it was puzzling that the radio core was not visible; our BIMA results confirm that there is a bright radio core at the galaxy center. Our observation of the flat spectrum core in NGC 3801 is thus consistent with the unification scheme for AGNs in radio loud galaxies.

4.2. The Central Molecular Gas Disk

As described in Section 3.2, CO clumps A and B appear associated with the dust filament at a PA of 24° that is offset about 1'' west of the nucleus. This filament resembles a disk seen nearly edge on (see Verdoes Kleijn et al 1999); if we take the distance of the peaks of clumps A and B from the nucleus ($\sim 10''$) as the radius of the disk, then the fact that the filament is offset $\sim 1''$ west of the nucleus suggests a disk with a 10/1 axis ratio, implying a disk with an inclination of 84° with the near side facing east. The position-velocity cut at

$PA = 24^\circ$ (Figure 9) is also consistent with a disk seen close to edge on. Both clumps A and B are offset from the nucleus by about 250 km s^{-1} , assuming a systemic velocity of 3451 km s^{-1} . The velocity gradient for the 2 kpc CO disk is in the same direction as the gradient seen in $\text{H}\alpha$ and [NII] on scales of a few hundred pc in STIS HST data by Verdoes Kleijn et al. (1999). If we interpret the velocity gradient as rotation, then with a nearly edge-on inclination of 84° the circular velocity is $v_c = 250 \text{ km s}^{-1}$ at a radius of 2.3 kpc ($10''$), which gives a rough estimate of the dynamical mass $M_{dyn} = v_c^2 r / G \approx 3 \times 10^{10} \text{ M}_\odot$. The combined molecular mass of CO clumps A and B is about $3 \times 10^8 \text{ M}_\odot$, about 1% of the dynamical mass within this radius. The HI seen in emission is at similar velocities to CO clumps A and B; if we attribute the HI emission to the same regions, then the mass in neutral atomic gas is $1.2 \times 10^9 \text{ M}_\odot$, about four times the molecular mass, and the total gas mass is about 5% of the dynamical mass.

The total molecular gas mass in NGC 3801 is lower than in most spiral galaxies but large compared to gas poor ellipticals. The molecular gas surface density in NGC 3801 averaged over the R_{25} radius is about $0.2 \text{ M}_\odot \text{ pc}^{-2}$, similarly small compared to most spirals (e.g. Sheth et al. 2002). For the molecular gas disk itself (e.g. clumps A and B), adopting a radius of 2.3 kpc the average face-on surface density is $18.4 \text{ M}_\odot \text{ pc}^{-2}$; this is large compared to the molecular surface density in the solar neighborhood but somewhat smaller than the average for the Milky Way at a radius of 5 kpc (i.e. including the 5 kpc ring).

We can place constraints on the star formation rate in NGC 3801 using the infrared luminosity of $2.4 \times 10^9 \text{ L}_\odot$ derived from the IRAS 60 and 100 μm fluxes (Knapp et al. 1989) using the relations given by Cox (1999). Using the relation $SFR = 4.5 \times 10^{-44} L_{FIR}$ (Kennicutt 1998) to derive the star formation rate (SFR), we obtain a $SFR \sim 0.4 \text{ M}_\odot \text{ yr}^{-1}$. We can also estimate the star formation rate using the $\text{H}\alpha + [\text{NII}]$ luminosity observed with HST by Verdoes Kleijn et al. (1999). Using the star formation relation for $\text{H}\alpha$ in Kennicutt (1998) and assuming all the luminosity is from $\text{H}\alpha$, we find a star formation rate of $0.2 \text{ M}_\odot \text{ yr}^{-1}$, a factor of two lower than the infrared estimate. It is possible that the optical estimate is affected by dust extinction in the edge-on disk. This is a fairly low SFR compared to the disks of nearby spiral galaxies, which have a SFR of a few $\text{M}_\odot \text{ yr}^{-1}$, but larger than gas poor ellipticals.

By contrast, the other FR I mapped at high resolution, 3C 31, has a more massive 10^9 M_\odot disk with a radius of about 1 kpc (Okuda et al. 2005). This yields a surface density of $300 \text{ M}_\odot \text{ pc}^{-2}$, larger even than the median for the central 500 pc radius of nearby spiral galaxies (Sakamoto et al. 1999; Sheth et al. 2002). Yet Okuda et al. (2005) note the absence of detected star formation in 3C 31, very different from NGC 3801.

Assuming a present rate of $SFR \sim 0.4 \text{ M}_\odot \text{ yr}^{-1}$, the molecular gas will last for $\sim 10^9 \text{ yr}$

before being exhausted by star formation. Including the HI reservoir, the gas can last for well over 10^9 yr.

4.3. Clump C: Infalling Molecular Gas

The nature of the eastern CO clump, clump C, is particularly intriguing. It does not appear to be associated with the central gas disk. If it were in that disk, because it is near the minor axis its deprojected distance from the nucleus would be 20 kpc, an order of magnitude further than clumps A and B. Also, it has emission in the range 3470 to 3630 km s^{-1} , significantly redshifted relative to the 3451 km s^{-1} systemic velocity; given that it would be on the disk minor axis, this velocity is highly non-circular. Assuming the disk orientation described in Section 3.2, it would be outflowing at an improbably large velocity. We conclude that it is not in the central gas disk.

Another possibility is that clump C is part of a second disk oriented perpendicular to the central disk. NGC 3801 is sometimes classified as an S0 galaxy, and the east filament partly associated with clump C might be the the dusty S0 disk seen edge on. However, the odds of encountering the specific geometry and orientations require are small, roughly one in a thousand. In detail, the “SO disk” would have to be edge-on to the line of sight to within less than 10° to explain the thinness of the filament, 2) the nuclear edge-on disk would have to be within 10° of edge-on and 3) the two disks would have to be perpendicular to each other to within 10° . More importantly, closer examination suggests that NGC 3801 is not an S0 galaxy: the isophotes beyond a radius of $30''$ are boxy (e.g. Heckman et al. 1999), consistent with a recent merger, and the inner isophotes show no evidence for a stellar disk that would be associated with an S0. Finally, we note that the gas in the two disks are on colliding orbits. If the eastern filament is an S0 disk it must have existed for some time. Yet the $PA = 24^\circ$ disk seems well established. Two disks with intersecting orbits cannot survive.

A third unlikely scenario is that the clump C gas was entrained from the central gas disk by the eastern AGN jet. This seems unreasonable first because the mass of clump C is comparable to the mass of disk itself; it is difficult to understand how such a large fraction of the disk could pass in the path of the jet. Also, at the end of Section 3.2 we presented strong evidence that the clump C is on the near side of the galaxy; in that case, if clump C is entrained from the central disk it should be blueshifted, contrary to our observations.

The most likely scenario is that clump C is gas resulting from a recent merger. Other evidence for a recent merger exists, such as the boxy stellar isophotes at radii larger than $30''$

(Heckman et al. 1996) and the warp in the $PA = 24^\circ$ dust disk evident in the HST V-band image of Verdoes Kleijn et al. (1999). As previously noted, clump C is associated with the eastern dust filament; the shape of this filament is consistent with the orbital path of tidally disrupted material. Molecular emission is only detected associated with the inner part of the filament. This may be because that is where the largest gas mass exists, or perhaps because the gas undergoes a transition to molecular form in the higher ISM pressure inner galaxy.

Since clump C must be on the near side of the galaxy and it is redshifted relative to the galaxy, we conclude that it is falling towards the galaxy. Its projected distance from the nucleus is only two or three kpc, and so it should soon interact with the 2 kpc nuclear disk.

4.4. The Role of Mergers in FR I and FR II Activity

There is considerable evidence that mergers fuel FR II radio sources, which are more energetic than FR I objects such as NGC 3801. Baum, Heckman, and van Breugel (1992) studied a sample of 40 radio galaxies. Using optical emission line studies, they concluded that all the FR II galaxies showed evidence for dynamically young gas disks acquired via mergers, and suggested that this plays a key role in the FR II phenomenon. There is also evidence for gas disks with abundant molecular gas in FR II sources. In particular, Evans et al. (1999) found that the FR II galaxy 3C 293 has an asymmetric gas disk with a molecular hydrogen mass of $1.5 \times 10^{10} M_\odot$. The gas is distributed over a 2.8 kpc radius region, and may constitute as much as 10% of the dynamical mass of the galaxy within that radius.

For the less energetic FR I galaxies, the suggestion has been that the AGN may be fueled by gas acquired from the intracluster medium via a cooling flow (e.g. Baum et al. 1992), motivated in part by the tendency for FR I galaxies to be found in clusters. However, our observations together with the recent Okuda et al. (2005) Nobeyama map of the FR I galaxy 3C 31 suggests that mergers in addition to cooling flow gas, is important for powering the AGN. The gas disk in NGC 3801 is three times less massive and has a surface density nearly a factor of 20 times lower. But it is nonetheless a significant amount of gas. Perhaps more significantly, in NGC 3801 there is abundant evidence that gas has recently arrived via a merger (e.g. clump C) and that the gravitational effects of the merger are significant (e.g. the warp in the dust disk, the asymmetric distribution of gas in the disk, and the boxy optical isophotes). Hence, it appears that mergers and the resultant gas inflow (especially gas in non-coplanar orbits) may also play a key role in the FR I phenomenon. Based on the limited high resolution studies so far, the gas masses (and the gas fraction relative to the dynamical mass) seem somewhat lower in FR I galaxies compared to FR II galaxies. However, observations of a larger sample of galaxies and at higher angular resolution will be

essential to understanding gas fueling in radio galaxies; such observations are expected soon with the CARMA millimeter-wave array.

4.5. Jet Entrainment of Molecular Gas?

Figure 7 shows that the projected eastern radio jet passes almost directly through clump C. This raises the question of whether the jet is in fact interacting with the molecular cloud or instead simply appears projected behind the CO cloud. Powerful supersonic jets, such as those found in FR II galaxies, overtake ambient clouds and inflate an overpressured cocoon in which the gas expands mostly perpendicular to the jet axis, driving a bow shock into the ambient gas (e.g. O’Dea et al. 2002; 2004). However, such expansion is not seen in clump C. The HI gas, which is seen in absorption and as previously discussed must be on the near side of the jet, has nearly the same velocity range as the CO gas. The similarity in velocity range argues against expansion such as produced by highly supersonic FR II jets (e.g. O’Dea et al. 2002, 2004). Thus the jet is not affecting the gross kinematics of the cloud.

A more likely possibility is jet entrainment (e.g. De Young 1986; Bicknell 1986). Note that earlier we ruled out the possibility that clump C is gas entrained from the nuclear disk; here we examine the possibility that the jet is entraining gas from clump C. Jet entrainment is thought to occur in transonic jets, such as those found in FR I galaxies. Here gas in the turbulent boundary layer along the edge of the jet is entrained and accelerated mainly along the direction of the jet flow. In this case, the kinematics of gas on the near side (e.g. HI in absorption) and the far side should not show a systematic difference. Thus, the velocities associated with clump C are consistent with entrainment. In fact, the position-velocity diagram for clump C shown in the lower panel of Figure 9 shows possible evidence supporting the entrainment picture. Note that the velocity of clump C becomes less redshifted with increasing distance from the nucleus. This is in the opposite sense of the gradient expected for a rising rotation curve. In principle, it could be explained as a declining rotation curve. However, the velocity decreases from about 3600 km s^{-1} at $7''$ from the nucleus to about 3540 km s^{-1} beyond $10''$ from the nucleus, much too large a decrease to be attributed to a declining rotation curve. However, the decreasing redshift with distance from the nucleus is in the correct direction expected for jet entrainment if the eastern jet is the approaching jet, as supported by our observations.

Figure 4 also shows that the eastern jet appears to bend just after appearing to pass through clump C, suggesting a possible association. We note, however that the opposite jet also bends at the same distance from the nucleus, but there is no detected molecular gas concentration. Such bends can occur due to interaction with the rotating ISM of a galaxy or

due to precession of the jet; we favor the latter interpretation since the one clear gas rotation axis in NGC 3801 (the $PA = 24^\circ$ disk) has the wrong orientation to attribute the jet bend to rotation of the ISM. The jet axis close to the nuclear disk is offset from normal to the disk by about 6° ; the offset is not surprising as the radio jets in nearby radio galaxies are not always normal to the large scale gas disk (e.g. Wilson, Yang & Cecil 2001; Verdoes Kleijn & de Zeeuw 2004). The inflow from the disk that presumably feeds the black hole can produce torques leading to jet precession.

Also we note the remarkable alignment of the eastern jet with the eastern dust filament, evident in Figure 6. The initial bend in the jet coincides almost exactly with a bend in the dust filament. Further from the galaxy the jet bends further to the north while the filament continues nearly in a straight line for more than $20''$ (4.6 kpc). This might suggest ballistic motion of the denser gas while the more diffuse radio gas bends to the north. However, given that the dense gas was entrained by the jet, it is difficult to understand how it can separate from the jet. Also, it is not obvious how the entrained gas could remain so collimated. Thus we prefer our earlier conclusion that the filament traces the orbital path of the tidally disrupted merging gas of clump C.

5. CONCLUSIONS

We have mapped and detected 3 mm continuum and CO (1–0) emission from the Fanaroff & Riley type I galaxy NGC 3801 using the BIMA array. We draw the following conclusions:

1. We detect 3 mm continuum emission from twin radio jets of similar brightness and extent and an unresolved nuclear core. Comparing to a VLA 20 cm map, we find that the 3 mm and 20 cm jets coincide, and derive a spectral index of -0.7 , consistent with synchrotron emission. The core has not previously been detected in the radio; we derive a 3 mm flux of 15 mJy, substantially brighter than the 20 cm upper limit of 0.8 mJy. The millimeter-wave spectrum is flat, as generally observed for the compact radio core of an AGN; other emission mechanisms appear unlikely. Our detection of the bright compact core, along with the twin jet structure, supports the idea that FR I galaxies are the parent population of BL Lac objects.
2. We mapped CO (1–0) emission in a region of roughly $100''$ (23 kpc) diameter and detect CO concentrated in three regions, each with molecular masses in excess of $10^8 M_\odot$ assuming the standard conversion factor for CO. Unresolved HI emission is seen over a similar velocity range. We are able to associate each of the CO clumps with an HI emission

or absorption component. The molecular mass is approximately 25% of the HI mass.

3. Two of the CO clumps are associated with a nearly edge-on dust disk imaged in previous HST V-band observations; the disk is oriented approximately perpendicular to the twin radio jets. The CO and dust distributions suggest an inhomogeneous disk (i.e. not axisymmetric) or ring with a radius of about 2.3 kpc. The velocity shift between the two regions and across one of the clumps is consistent with rotation reaching a maximum of 250 km s^{-1} . We infer an inclination of 84° from the offset of the dust major axis from the nucleus relative to the radius of the disk or ring. The implied dynamical mass is about $3 \times 10^{10} \text{ M}_\odot$; thus the molecular mass is approximately 1% of the dynamical mass.

4. We find evidence that the other CO region, clump C, is infalling gas from a recent merger. Perhaps most intriguing, there are suggestions that one of the radio jets is entraining material from the clump.

5. There are abundant signs that NGC 3801 has undergone a recent minor merger. These include the infalling gas, boxy optical isophotes, the structure of the dust filaments, and the inhomogeneous distribution of gas. We therefore suggest that, as in F-R II galaxies, mergers play a role in the F-R I phenomenonon.

We thank S. White for very useful discussions, especially regarding the VLA data. Conversations with E. Ostriker, C. Reynolds, and J. Stone were very helpful. We thank the referee for many very constructive comments. Observations with the BIMA millimeter-wave array are partially supported by NSF AST-0228974. This research has made use of the NASA/ IPAC Infrared Science Archive, which is operated by the Jet Propulsion Laboratory, California Institute of Technology, under contract with the National Aeronautics and Space Administration.

REFERENCES

Baum, S. A.; Heckman, T. M.; van Breugel, W. 1992, ApJ, 389, 208

Blandford, R. D. 1984, in 11th Texas Symposium on Relativistic Astrophysics, 11th, Austin, New York Academy of Sciences, Annals (ISSN 0077-8923), vol. 422, 1984, p. 303-318

Blandford, R. D. & Konigl, A. 1979, ApJ, 232, 34

Caproni, A. & Abraham, Z. 2004, ApJ, 602, 625

Cox, A.N. 1999, in Allen's Astrophysical Quantities, Springer Verlag

Duprie, K. & Schneider, S. E. 1996, AJ, 112, 937

Eckart, A.; Cameron, M.; Rothermel, H.; Wild, W.; Zinnecker, H.; Rydbeck, G.; Olberg, M.; Wiklind, T. 1990, ApJ, 363, 451

Evans, A. S.; Sanders, D. B.; Surace, J. A.; Mazzarella, J. M. 1999a, ApJ, 511, 730

Evans, A. S.; Kim, D. C.; Mazzarella, J. M.; Scoville, N. Z.; Sanders, D. B. 1999b, ApJL, 521, 107

Fanaroff, B. L. & Riley, J. M. 1974, MNRAS, 167, 31

Fabian, A. C.; Sanders, J. S.; Allen, S. W.; Crawford, C. S.; Iwasawa, K.; Johnstone, R. M.; Schmidt, R. W.; Taylor, G. B. 2003, MNRAS, 344L, 43

Giovannini, G.; Taylor, G. B.; Feretti, L.; Cotton, W. D.; Lara, L.; Venturi, T. 2005, ApJ, 618, 635

Ghisellini, G. & Maraschi, L. 1989, ApJ, 340, 181

Hardcastle, M. J. & Looney, L. W. 2001, MNRAS, 320, 355

Hardee et al 1994, ApJ, 424, 126

Heckman, T. M.; Balick, B.; van Breugel, W. J. W.; Miley, G. K. 1983, AJ, 88, 583

Heinz, S.; Reynolds, C.S.; Begelman, M.C. 1998, ApJ, 501, 126

Helfer, T.T.; Vogel, S.N.; Lugten, J.B.; Teuben, P.J. 2002, PASP, 114, 350

Helfer, T.T.; Thornley, M.D.; Regan, M.W.; Wong, T.; Sheth, K.; Vogel, S.N.; Blitz, L.; Bock, D.C.-J. 2003; ApJS, 145, 259

Inoue, M. Y.; Kameno, S.; Kawabe, R.; Inoue, M.; Hasegawa, T.; Tanaka, M. 1996, AJ, 111, 1852

Jarrett, T. H.; Chester, T.; Cutri, R.; Schneider, S. E.; Huchra, J. P. 2003, AJ, 125, 525

Jones, D.L.; Wehrle, A.E.; Piner, B.G.; Meier, D.L. 2001, ApJ, 553, 968

Kennicutt, R. C. 1998, ARA&A, 36, 189

Knapp, G. R.; Guhathakurta, P.; Kim, D.; Jura, Michael A. 1989, ApJS, 70, 329

Knapp, G. R.; Rupen, M. P. 1996 ApJ, 460, 271

Krolik, J.H. 1999, Active Galactic Nuclei, Princeton University Press

Lees, J. F.; Knapp, G. R.; Rupen, M. P.; Phillips, T. G. 1991, ApJ, 379, 177

Lim J.; Leon, S.; Combes, F.; Dinh-v-Trung 2003, in Active Galactic Nuclei: from Central Engine to Host Galaxy, eds S. Collin, F. Combes and I. Shlosman, ASP, Vol. 290, p. 529.

Lim, J.; Leon, S.; Combes, F.; Dinh-V-Trung 2000, ApJL, 545, 93

Leon, S.; Lim, J.; Combes, F.; Dinh-v-Trung 2003, in Active Galactic Nuclei: from Central Engine to Host Galaxy, eds S. Collin, F. Combes and I. Shlosman, ASP, Vol. 290, p. 525

Looney, L.W. & Hardcastle, M.J. 2000 ApJ, 534, 172

Marscher, A. P. 1980, ApJ, 235, 386

Mazzarella, J. M.; Graham, J. R.; Sanders, D. B.; Djorgovski, S. 1993, ApJ, 409, 170

Merritt & Ekers 2002, Science 297, 1310

Mirabel, I. F.; Sanders, D. B.; Kizes, I. 1989, ApJ, 340L, 9

O'Dea, C. P.; Baum, S. A.; Mack, J.; Koekemoer, A. M.; Laor, A. 2004, ApJ, 612, 131

O'Dea, C. P.; de Vries, W. H.; Koekemoer, A. M.; Baum, S. A.; Morganti, R.; Fanti, R.; Capetti, A.; Tadhunter, C. N.; Barthel, P. D.; Axon, D. J.; Gelderman, R. 2004, AJ, 123, 2333

Okuda, T. Kohno, K.; Iguchi, S.; Nakanishi, K. 2005, ApJ, 620, 673

Parma, P.; Murgia, M.; Morganti, R.; Capetti, A.; de Ruiter, H. R.; Fanti, R. 1999, A&A, 344, 7

Phillips, T. G.; Ellison, B. N.; Keene, J. B.; Leighton, R. B.; Howard, R. J.; Masson, C. R.; Sanders, D. B.; Veidt, B.; Young, K. 1987, ApJ, 322L, 73

Reynolds, C.S.; Brenneman, L.W.; Stocke, J.T 2005, MNRAS, 357, 381

Rudnick, L.; Jones, T. W.; Fiedler, R. 1986, AJ, 91, 1011

Rybicki, G. & Lightman, A.P. 1979, Radiative Processes in Astrophysics (New York: John Wiley & Sons)

Sakamoto, K.; Okumura, S. K.; Ishizuki, S.; Scoville, N. Z 1999, ApJ, 525, 691

Salter, C. J.; Chini, R.; Haslam, C. G. T.; Junor, W.; Kreysa, E.; Mezger, P. G.; Spencer, R. E. et al. 1989, A&A, 220, 42

Sault, R. J.; Teuben, P. J.; Wright, M. C. H. 1995, ADASS, ASP Conference Series, Vol. 77, eds. R.A. Shaw, H.E. Payne, and J.J.E. Hayes, p. 433.

Schmitt et al 2002, *ApJ*, 575, 150

Scoville, N. Z.; Sanders, D. B. 1987, in *Interstellar processes*, ed. D. Hollenbach & H. Thronson (Dordrecht, D. Reidel), p.21

Sheth, K.; Vogel, S.N.; Regan, M.W.; Teuben, P.J.; Harris, A.I.; Thornley, M.D. 2002, *AJ*, 124, 2581

Strong, A. W. et al. 1988, *A&A*, 207, 1

Trussoni, E.; Capetti, A.; Celotti, A.; Chiaberge, M.; Feretti, L. 2003, *A&A*, 403, 889

Turner, J.L. & Ho, P.T.P. 1983, *ApJL*, 268, L79

Urry, C. M.; Padovani, P. 1995, *PASP*, 107, 803

Verdoes Kleijn, Gijs A.; Baum, Stefi A.; de Zeeuw, P. Tim; O'Dea, Chris P. 1999, *AJ*, 118, 2592

Verdoes Kleijn, Gijs A.; de Zeeuw, P.T. 2004, *A&A* submitted

Walker, R. C.; Dhawan, V.; Romney, J. D.; Kellermann, K. I.; Vermeulen, R. C. 2000, *ApJ*, 530, 233

Wegner, G.; Bernardi, M.; Willmer, C. N. A.; da Costa, L. N.; Alonso, M. V.; Pellegrini, P. S.; Maia, M. A. G.; Chaves, O. L.; Rit, C. 2003; *AJ*, 126, 2268

Welch, W.J. et al. 1996, *PASP*, 108, 93

Wiklind, T.; Combes, F.; Henkel, C. 1995, *A&A* 297, 643

Wilson, A. S.; Yang, Y.; Cecil, G. 2001, *ApJ*, 5560, 689

Wolfire, M.G. & Churchwell, E. 1994, *ApJ*, 427, 889

Wright, M. & Birkinshaw, M. 1984, *ApJ*, 281, 135

Wrobel, J.M. & Condon, J. J 1989, VLA Archive

Young, L.M. 2002, *AJ*, 124, 788

Xu, C.; Baum, S. A.; O'Dea, C. P.; Wrobel, J. M.; Condon, J. J 2000, *AJ*, 120, 2950

Table 1. Parameters of NGC 3801

Parameter	Value	Reference
Galaxy Type	S0/a	1
Galaxy Position (RA, DEC)	$11^h 40^m 16^s.9$, $17^\circ 43' 40.5''$	1
Other Names	UGC 06635, 4C +17.52	1
Velocity & Redshift	3451 km s^{-1} , 0.011	2,1
Linear Distance Scale	0.23 kpc/arcsec	...
PA of Dust Lane	$24^\circ \pm 2^\circ$	3
PA of Radio Jets	120°	4

Table 2. Results of Continuum Observations of NGC 3801

Parameter	Value
Peak Flux of Core at 86.5 GHz (mJy/beam)	15.1 ± 1.6
Peak Flux of Core at 110.2 GHz (mJy/beam)	10.6 ± 1.9
Peak Flux of Core at 112.4 GHz (mJy/beam) (beam= $13.0'' \times 7.5''$)	15.5 ± 1.5
Position of Radio Core (RA, DEC)	11:40:16.9, +17:43:41
Flux in Radio Core (mJy)	15
Flux in Radio Lobes (mJy)	36
Total Flux (mJy)	51
P.A. of Radio Lobes	20°
Length of Radio Lobes	$\sim 35''$

Table 3. Results of CO Observations of NGC 3801

Parameter	Value
Total CO Flux (Jy km s ^{−1})	14.2
CO Flux of Clump A	3.8
CO Flux of Clump B	5.0
CO Flux of Clump C	5.3
CO total line width (km s ^{−1})	500
Rotational velocity of gas disk (km s ^{−1})	250
P.A. of Gas Disk	24°
Total Molecular Gas Mass $M(H_2)$ (M_\odot)	4.9×10^8
Ratio of molecular to dynamical mass $M(H_2)/M_{dyn}$	0.015

Figure Captions

Figure 1. BIMA maps of 2.7 mm continuum emission in NGC 3801; emission is averaged over the upper and lower sidebands, with a mean frequency of 112.4 GHz. The “X” marks the 2MASS near-infrared position for the nucleus. The beam is shown in the lower left of each panel. (a) The left panel shows a map with natural weighting for maximum sensitivity, which yields a beam size of $12'' \times 10''$. The peak is $20.9 \text{ mJy beam}^{-1}$ and the noise level is $1.1 \text{ mJy beam}^{-1}$. Emission is contoured at 3, 6, 9, 12, 15, and 18 times the rms noise level, with negative contours dashed. (b) The right panel shows a map with robust = 0.5 weighting, giving better resolution. The beam size is $10'' \times 8''$. The peak is $18.0 \text{ mJy beam}^{-1}$ and the noise level is $1.4 \text{ mJy beam}^{-1}$. Emission is contoured at 2, 4, 6, 8, 10, and 12 times the noise level.

Figure 2. (Upper left) Map of 20 cm (1.5 GHz) radio continuum emission from NGC 3801 obtained in the VLA A array by Wrobel & Condon (1989). The map has a beam size of $1.5 \times 1.5''$ (indicated in lower left) and is contoured at intervals of 2, 4, 8, 16, and 32 mJy beam^{-1} . The 2MASS near-IR position for the nucleus is indicated by the X in this and all panels. (Upper right) Map of 20 cm radio continuum obtained in the VLA B array. The map has been convolved to a resolution of $10 \times 8''$ to match the resolution of the BIMA 2.7 mm map shown in the right of Figure 1. The map is contoured at intervals of 30, 60, 120, and $240 \text{ mJy beam}^{-1}$. (Lower left) Spectral index map formed from the $10 \times 8''$ 20 cm and 2.7 mm maps is shown as greyscale. The greyscale is a square-root stretch from -0.9 (white) to 0 (black). The black lines show spectral index contours at -0.8 , -0.7 , and -0.6 . Most of the area of each lobe has a spectral index between -0.8 and -0.7 . The white contours are the same contours as shown in the $10 \times 8''$ 20 cm map. (Lower right) Map of 2.7 mm continuum emission after subtracting emission from the radio jets, as described in the text. Contours are at 27.5 , 55 , 82.5 , 110 , and $137 \text{ mJy beam}^{-1}$.

Figure 3. Map of velocity-integrated emission in the CO (1–0) line in NGC 3801 obtained with BIMA. The contours are at 2, 3, 4, and 5 times the rms noise level, which is $13 \text{ Jy beam}^{-1} \text{ km s}^{-1}$. The $12'' \times 10''$ beam is shown in the lower left. The 2MASS position for the nucleus is marked with an X. The three peaks in CO (1–0) emission are marked as A, B, and C.

Figure 4. Contours of BIMA 2.7 mm continuum emission overlaid on a greyscale image of VLA 20 cm emission. The continuum emission is contoured as in Figure 1a.

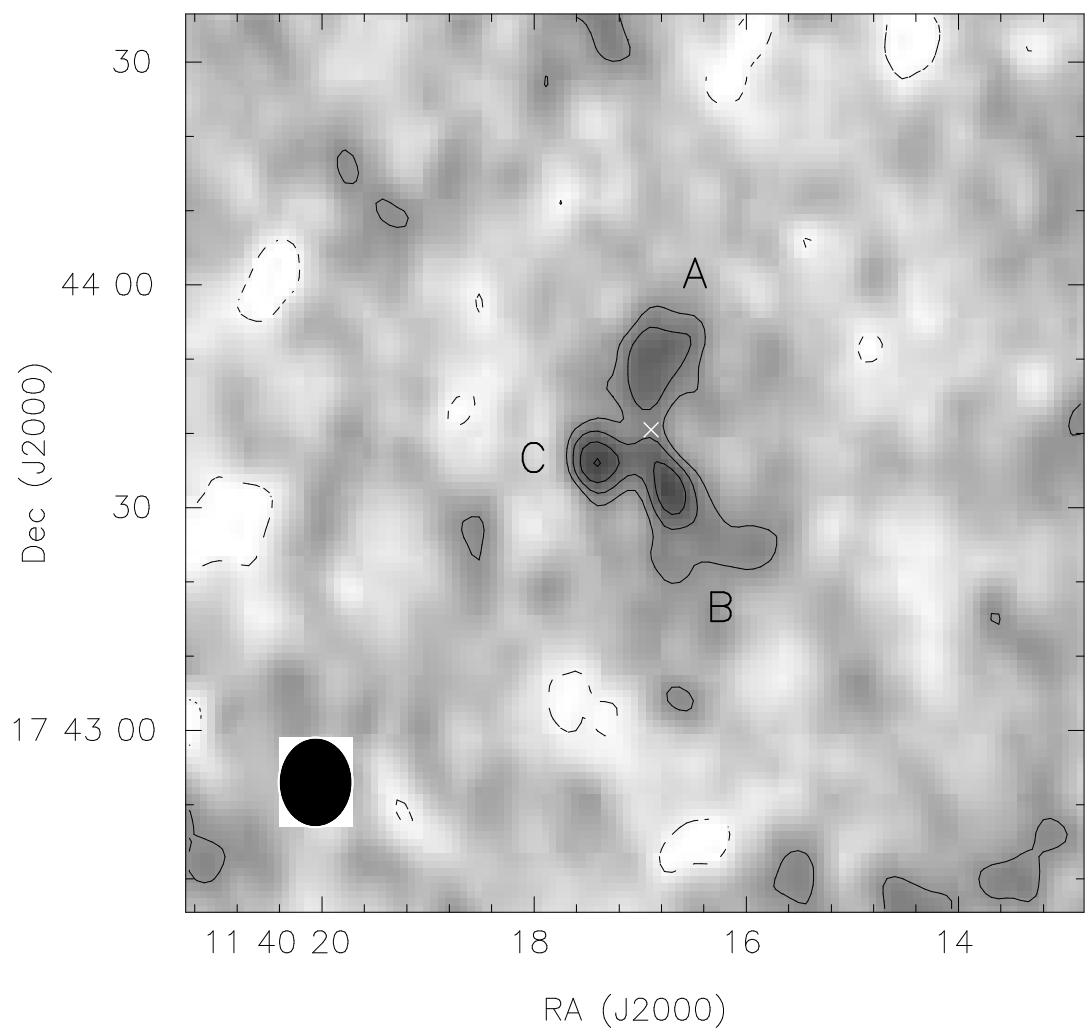
Figure 5. BIMA spectrum of CO (1–0) emission in NGC 3801 summed over a $30 \times 40''$ box.

Figure 6. VLA 20 cm radio continuum (upper panel) and BIMA velocity-integrated CO (1–0) emission (lower panel) overlaid on HST F555W image of NGC 3801. The 20 cm and CO (1–0) images are contoured as in Figures 2 and 3, respectively. The HST image has been processed to remove the radial gradient in light from the host galaxy so as to better reveal dust features. The galaxy nucleus is marked with an X.

Figure 7. Contours of BIMA CO (1–0) velocity-integrated emission overlaid on a greyscale image of VLA 20 cm emission. CO emission is contoured as in Figure 3.

Figure 8. Flux of the radio continuum core in NGC 3801 as a function of frequency at millimeter-wavelengths on a log-log plot. One σ error bars are shown. The dotted line shows a $\nu^{3.5}$ power law characteristic of dust emission, which is ruled out. The millimeter-wave spectrum can be fitted by a flat spectrum.

Figure 9. Position-velocity (PV) plots of CO (1–0) emission for two cuts passing through the nucleus of NGC 3801. The upper panel shows the cut at $\text{PA} = 24^\circ$ corresponding to the major axis of the nuclear disk; the lower panel shows the perpendicular direction ($\text{PA}=114^\circ$). The systemic velocity is indicated by the dotted line. Contours are at 14 , 21 , and 28 mJy beam^{-1} . The $\text{PA}=24^\circ$ cut passes through CO clumps A and B, which are labeled. The $\text{PA}=114^\circ$ cut passes through clump C.

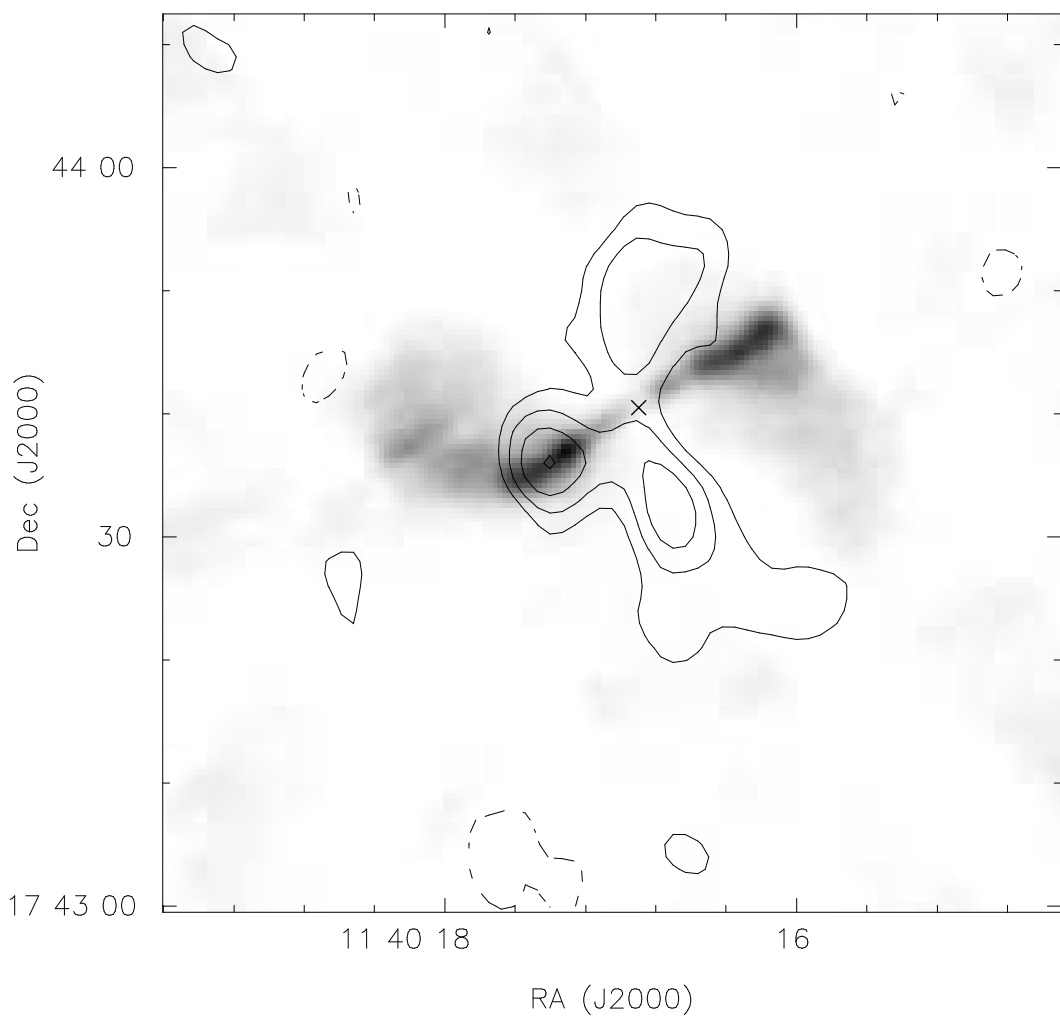


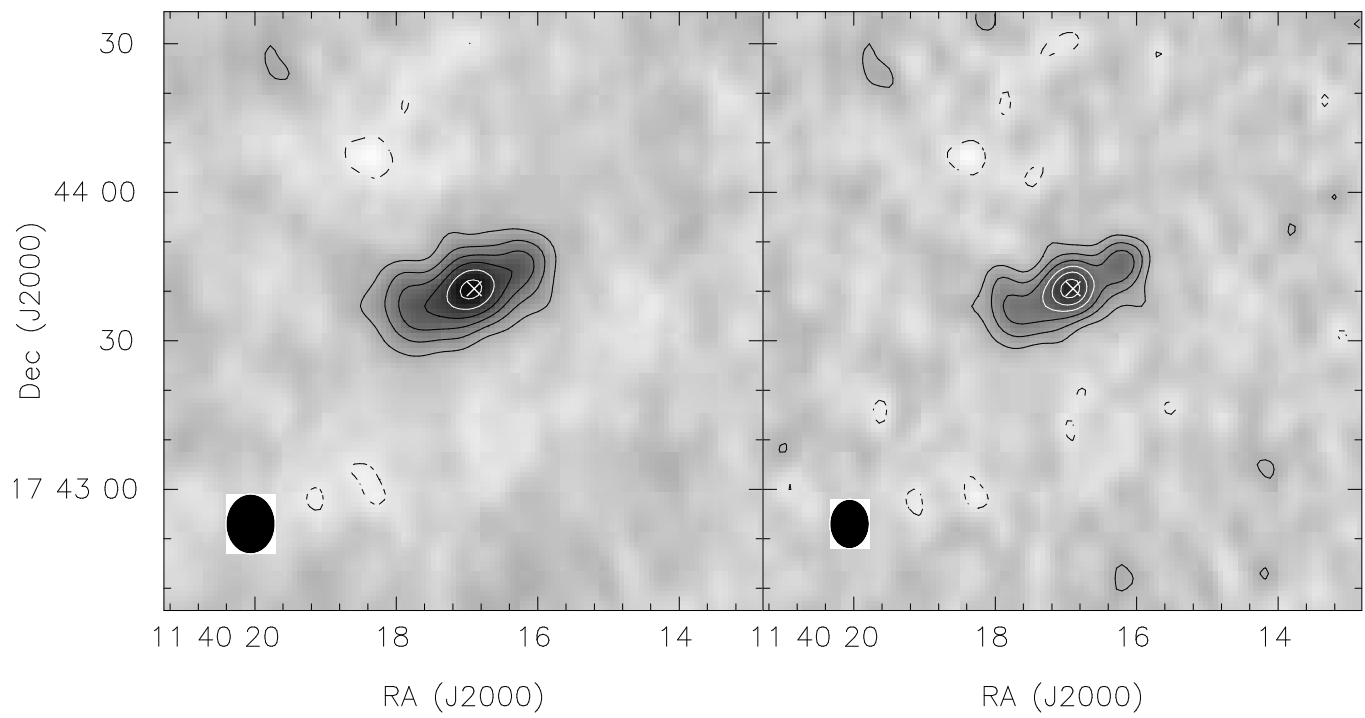
This figure "HST_overlay_BW.gif" is available in "gif" format from:

<http://arxiv.org/ps/astro-ph/0505285v1>

This figure "cm_maps.gif" is available in "gif" format from:

<http://arxiv.org/ps/astro-ph/0505285v1>





This figure "mm_on_vla.gif" is available in "gif" format from:

<http://arxiv.org/ps/astro-ph/0505285v1>

